# Operation modes of the molecular motor kinesin

S. Liepelt and R. Lipowsky

*Max Planck Institute of Colloids and Interfaces, Science Park Golm, 14424 Potsdam, Germany* [*]

(Received 30 July 2008; revised manuscript received 16 December 2008; published 22 January 2009)

The velocity and the adenosine triphosphate (ATP) hydrolysis rate of the molecular motor kinesin are studied using a general network representation for the motor, which incorporates both the energetics of ATP hydrolysis and the experimentally observed separation of time scales between chemical and mechanical transitions. Both the motor velocity and its hydrolysis rate can be expressed as superpositions of excess fluxes for the directed cycles (or dicycles) of the network. The sign of these dicycle excess fluxes depends only on two thermodynamic control parameters as provided by the load force $F$ and the chemical energy $\Delta\mu$ released during the hydrolysis of a single ATP molecule. In contrast, both the motor velocity and its hydrolysis rate depend, in general, on the load force $F$ as well as on the three concentrations of ATP, adenosine diphosphate (ADP), and inorganic phosphate (P), separately. Thus, in order to represent the different operation modes of the motor in the $(F, \Delta\mu)$ plane, one has to specify two concentrations such as the product concentrations [ADP] and [P]. As a result, we find four different operation modes corresponding to the four possible combinations of ATP hydrolysis or synthesis with forward or backward mechanical steps. Our operation diagram implies in particular that backward steps are coupled to ATP hydrolysis for sufficiently large ATP concentrations, but to ATP synthesis for sufficiently large ADP and/or P concentrations.

## I. INTRODUCTION

The performance of molecular motors is intimately related to their enzymatic activity. Chemical reactions, which change the chemical composition of the enzyme-ligand compound, are coupled to conformational changes of the motor molecule [1–3]. One example is provided by the kinesin molecule, which generates force and directed motion against an opposing load using the energy gained by catalyzing the hydrolysis of adenosine-triphosphate (ATP) to adenosine-diphosphate (ADP) and an inorganic phosphate group (P). In the present article, we address this energy transduction by the kinesin motor using a network representation first introduced in [4,5].

Kinesin is a motor molecule that consists of two identical amino acid chains dimerized in a coiled coil; see, e.g., review in [6]. One end of the protein dimer binds to cell organelles, such as small vesicles or mitochondria, while at the other end, each of the two chains forms a globular head-domain, which is able to bind to microtubules, which represent rather rigid and polar cytoskeletal filaments [7,8]. These motor heads do not only mediate the binding of kinesin to the microtubule track, but also contain a binding pocket for ATP, which is also the catalytic site for ATP hydrolysis [9,10]. The content of the nucleotide binding pocket affects the microtubule binding affinity of the motor head [11,12], which turns out to be crucial for the coordination of the two motor heads leading to a remarkable high processivity of about 100 successive unidirectional steps [13]. Each individual motor step of kinesin is coupled to the hydrolysis of exactly one ATP molecule [14] and displaces the center of mass by 8 nm. During this displacement, the trailing head moves twice this length—i.e., 16 nm—towards the microtu-

bule plus end to become the new leading head [14–16]. Molecular details of the gating mechanism that enables communication between the two heads are still a matter of debate [17–21]. Since the catalytic reactions of molecular motors are directly coupled to mechanical displacement, its kinetics can be observed at the single molecule level. For the kinesin motor, e.g., the mean velocity, randomness, run length, and fraction of forward to backward steps have been measured [22–25]. These observations of the motor dynamics complement biochemical measurements of nucleotide binding and release rates [26–29].

The coupling to unbalanced ATP hydrolysis keeps the motor molecule out of equilibrium. In the following, we will consider nonequilibrium steady states, which apply as long as the environment of the motor changes slowly compared to its run time. In fact, the environment can be characterized by a fixed set of constant thermodynamic variables that consists of the temperature, the load force acting on the motor molecule, and the concentrations of ATP, ADP, and P in the solution as described previously in [30].

Therefore, the dynamics of the kinesin motor depends, for fixed temperature, on four thermodynamic control parameters: the load force and the three concentrations of ATP, ADP, and P. The latter concentration dependence is clearly demonstrated by the experimental observations in Ref. [23]. As explained in Ref. [30], all previous theoretical studies of kinesin were limited to certain subspaces of this four-dimensional parameter space. In addition, previous models were also restricted to unicycle models—i.e., to models with a single motor cycle; see, e.g., [23,27,29]. Unicycle models are, however, not capable of explaining the experimental results obtained in Refs. [24,25] on backward stepping.

Indeed, for a motor with a single cycle, backward stepping is always coupled to ATP synthesis, in which ADP and P are combined into ATP. However, for the bead assays used in [24,25], the ADP and P concentrations were rather low and, thus, were not able to reverse ATP hydrolysis as already

pointed out in Ref. [4]. This argument is rather general and directly shows, without any further assumptions, that the experimental observations on kinesin cannot be adequately described by unicycle models.

In [4], we introduced a six-state network to explain the possibility of backward stepping without the need to reverse ATP hydrolysis. The six-state network involves two distinct chemomechanical pathways, corresponding to forward and backward stepping, respectively, both of which are coupled to ATP hydrolysis. For small loads, the forward-stepping cycle carries a larger probability flux than the backward-stepping cycle. Consequently, the kinesin motor will effectively move forward. This changes, if the load force is increased, which does, however, not lead to a simple reversal of the forward-stepping cycle. Instead, the dominant reaction pathway changes and now becomes the backward-stepping cycle.

We found this six-state network model to be appropriate for describing the motor velocity and the fraction of observed forward to backward steps as well as the randomness parameter as a function of load force and ATP concentration, as long as we considered small concentrations of ADP and P. Comparison of the calculated inhibition of the motor velocity by ADP with experimental observations made it necessary to extend the network by one additional motor state [4]. The resulting network representation of the kinesin motor involves seven motor states and describes all experimentally observed properties of kinesin's processive motion and their dependences on the load force and the three concentrations of ATP, ADP, and P.

Since catalytic processes correspond to closed-state space trajectories of the corresponding enzyme, the cycles of the state space network play an essential role for the discussion of the motor dynamics [5,30]. This aspect has been worked out in great detail by Hill [31] for biochemical processes that do *not* involve mechanical work. In the present context, the decomposition of the local fluxes in form of nonlocal cyclic fluxes allows us to relate the motor kinetics to the thermodynamics of the energy transduction process. In our previous work, we established cyclic energy balance conditions for the transition rates, which follow from the requirements of thermodynamic consistency [5,30]. This energy balance ensures that the dynamics follows, on average, all chemomechanical cycles in the direction of heat release, in agreement with the second law of thermodynamics. Furthermore, the amount of released heat can be used to quantify the degree of irreversibility for the corresponding cycle. For reaction pathways that are not closed, the energy transduction process is incomplete and the heat release cannot be defined without the explicit knowledge of the intramolecular energy storage.The cyclic energy balance as derived in our previous studies also provides a connection to recent studies of entropy production in stochastic dynamics [32,33].

In the present article, the cyclic energy balance is used to determine the different operation modes of kinesin. These operation modes are defined with respect to two essential motor properties: the velocity and the hydrolysis rate of the motor. As shown below, both quantities can be expressed as superpositions of excess fluxes for the directed cycles (or dicycles) of the network. The sign of these dicycle excess fluxes depends only on the load force $F$ and the chemical energy $\Delta\mu$ released during the hydrolysis of a single ATP molecule. In contrast, both the motor velocity and its hydrolysis rate depend, in general, on the load force $F$ as well as on the three concentrations of ATP, ADP, and P, separately. Thus, in order to represent the different operation modes of the motor in the $(F, \Delta\mu)$ plane, one has to specify two concentrations such as the product concentrations [ADP] and [P]. As a result, we find four different operation modes corresponding to the four possible combinations of ATP hydrolysis or synthesis with forward or backward mechanical steps. Our operation diagram implies in particular that backward steps are coupled to ATP hydrolysis for sufficiently large ATP concentrations, but to ATP synthesis for sufficiently large ADP and P concentrations.

Our article is organized as follows. In Sec. II we define the state space and the network representation of the kinesin motor molecule. In Sec. III the network kinetics is described in terms of excess probability fluxes on dicycles. One important property of these dicycle excess fluxes is that their sign is completely determined by the released heat and, thus, by thermodynamics. Finally we show in Sec. IV how the interplay of the dicycle excess fluxes determines the operation modes of the kinesin motor. The main results of this article are explicit expressions for the stall force and the balancing chemical potential difference, which separate forward-backward stepping and ATP hydrolyzing-synthesizing modes, respectively. This analysis explicitly illustrates the dependence of the motor dynamics on both thermodynamic variables and kinetic model parameters.

## II. NETWORK REPRESENTATIONS OF THE KINESIN MOTOR

### A. Motor states connected by chemical and mechanical transitions

An individual catalytic reaction of ATP hydrolysis on a kinesin motor head involves the binding of the substrate ATP, the chemical cleavage, and finally the release of the products P and ADP. Since P is released very quickly after the decay [28], a motor head will be found in an empty ($E$), a bound ATP ($T$), or a bound ADP ($D$) conformation. The different states of the motor head have different binding affinities to the microtubule: namely, strongly bound $E$ and $T$ heads and weakly bound $D$ heads [11,12]. Single-molecule experiments [16,24] indicated that the 16-nm translation of the trailing head in the hand-over-hand stepping is fast compared to the overall catalytic turnover of ATP hydrolysis. Because of this separation of time scales, we will ignore conformational states of the kinesin molecule, which do not have a 8-nm-separated leading and trailing head. As a result, the conformational state space for the dimeric kinesin molecule includes nine states, as shown in Fig. 1.

We distinguish two types of transitions between these states. Chemical transitions correspond to changes in the composition of the motor heads. During these transitions, ATP, ADP, or P molecules are exchanged between motor and particle reservoirs of constant concentration. Note that in the kinesin network considered here, we have combined the
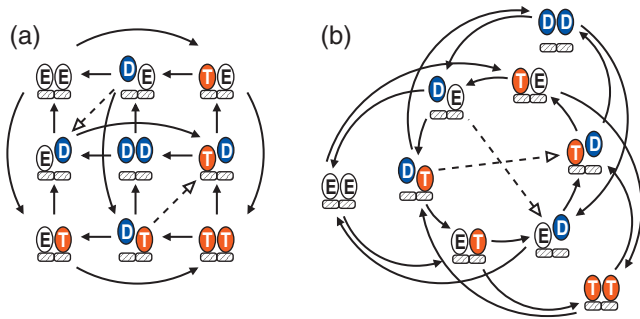
FIG. 1. (Color) (a)+(b) Two different representations of the nine-state network for dimeric kinesin, as defined via the composition of the two catalytic motor domains. A head with bound ATP or ADP is labeled $T$ or $D$, respectively. Empty heads are denoted by $E$. Both the $E$ and $T$ states are strongly bound to the microtubule, whereas the $D$ state is only relatively weakly attached as indicated by the small gap between the $D$ heads and the filament segments. All transitions between states are bidirectional; the direction of ATP hydrolysis, which consists of substrate (ATP) binding and product (ADP+P) release, is indicated by arrows. The two possible mechanical transitions are shown as dashed lines. Considering the right and left heads as being the leading and trailing heads, respectively, the open arrows at the mechanical transitions point in the direction of forward stepping.

cleavage of bound ATP to bound ADP+P with the subsequent P release [4]. Mechanical transitions represent displacements of the motor molecule, which performs mechanical work whenever an external load force acts against this directed motor movement. The process of an 8-nm step of the center of mass is identified with the 16-nm displacement of the trailing head, consistent with the hand-over-hand mechanism of processive kinesin. In the state space network of dimeric kinesin, a stepping transition (dashed lines in Fig. 1) has the effect of interchanging the position of the leading and the trailing head.

The high processivity of kinesin indicates that stepping originates from a state in which the leading and trailing heads are strongly and weakly bound, respectively [4]. This asymmetry is particularly pronounced for the inner "out-of-phase" cycle in Fig. 1(b), corresponding to the closed chemical pathway, in which the two motor heads do not appear with identical composition. For this closed chemical pathway, one can consider, in principle, two different mechanical transitions: (i) from state $DE$ to state $ED$ and (ii) from state $DT$ to state $TD$. Since the stepping transition from state $DE$ to state $ED$ competes with the ATP binding from $DE$ to $DT$, such a mechanical transition should lead to a reduction in the motor velocity for large ATP concentrations, which has not been observed experimentally. Thus, we take the stepping transition from $DT$ to $TD$ to be the dominating one.

For simplicity, we first focused on the six-state model, provided by the out-of-phase cycle of chemical transitions and the $DT$ to $TD$ stepping transition [4]. However, the strong reduction of the motor velocity by an increase of the ADP concentration makes it necessary to include the state $DD$ into the network description. In this way, we arrive at the seven-state network shown in Fig. 2 [4]. This seven-state network has six cycles, which describe four processes: (i)
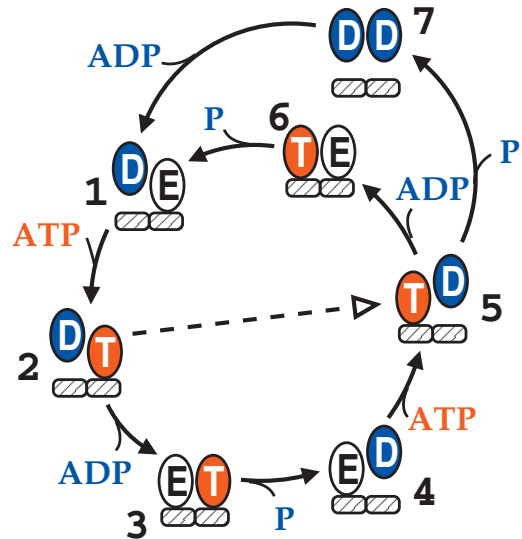


FIG. 2. (Color) Seven-state network for kinesin, which is consistent with all observations of its processive motion [4,30]. The arrows indicate the direction of ATP hydrolysis and forward stepping.

two dicycles $\mathcal{F}_1^+=|12561\rangle$ and $\mathcal{F}_2^+=|12571\rangle$ couple ATP hydrolysis to forward stepping, (ii) one dicycle $\mathcal{B}^+=|45234\rangle$ couples ATP hydrolysis to backward stepping, (iii) two dicycles $\mathcal{D}_1^+=|1234561\rangle$ and $\mathcal{D}_2^+=|1234571\rangle$ represent futile ATP hydrolysis without any stepping, and (iv) one dicycle $\mathcal{S}^+=|71657\rangle$ contains neither net hydrolysis nor stepping. While the cycles in (i) and (ii) are chemomechanical cycles that couple chemical and mechanical processes in one catalytic cycle, (iii) and (iv) can be classified as dissipative and thermal slip cycles, respectively [30].

### B. Motor dynamics and transition rates

The dynamics of the motor molecule will be described by a continuous time Markovian jump process on the seven-state network. This process is characterized by exponentially distributed dwell times $\tau_i$ with average values $\langle \tau_i \rangle$ for each state and jump probabilities $\pi_{ij}$ for each transition, with $\Sigma_j \pi_{ij}=1$. Together, these quantities define the transition rates $\omega_{ij}=\pi_{ij}/\langle \tau_i \rangle$. Each individual transition carries a local excess flux as given by

$$\Delta J_{ij} = P_i \omega_{ij} - P_j \omega_{ji}, \qquad (1)$$

where $P_i$ is the occupation probability of state $i=1,2,\ldots,7$. At steady state, the probabilities $P_i$ satisfy seven linear equations that represent the flux balance in each state, $\Sigma_j \Delta J_{ij}=0$. The transition rates $\omega_{ij}$ depend on the load force $F$ acting on the motor molecule and on the ATP, ADP, and P concentrations in the solution. In general, each transition rate can be written as

$$\omega_{ij} = \omega_{ij,0} \Phi_{ij}(F) \quad \text{with } \Phi_{ij}(0) = 1, \qquad (2)$$

where $\omega_{ij,0}$ is the rate in the load free case and $\Phi_{ij}(F)$ the force-dependent factor [5]. Here and below, the load force $F$ represents the force component tangential to the filament. In

general, the transition rates $\omega_{ij}$ may also depend on the force component perpendicular to the filament as discussed in [30], but the motor does not perform work against these perpendicular components.

If the transition $|ij\rangle$ involves binding of species $X$ (=ATP, ADP, or P), we take the binding rate to be proportional to the concentration of $X$—i.e., $\omega_{ij,0} = \kappa_{ij}[X]$. The reverse transition $|ji\rangle$ corresponds to the release of $X$. Both the mechanical stepping transitions and the release transitions do not depend on [ATP], [ADP], or [P] and are simply given by the rate constant $\omega_{ij,0} = \kappa_{ij}$. In [4,37], we determined the transition rate constants $\kappa_{ij}$ and load factors $\Phi_{ij}$ systematically from the experimental data in [22–25].

The environmental variables as given by load force $F$ and concentrations [ATP], [ADP], and [P] determine the dynamics of the motor—i.e., its velocity and hydrolysis rate via the $F$-dependent factors $\Phi_{ij}$ and the concentration-dependent zero-load rates $\omega_{ij,0}$. The second ingredient for the description of the motor dynamics is the topology of the underlying seven-state network, which can be characterized in terms of the different motor cycles as explained in the next section.

## III. DICYCLE EXCESS FLUXES

### A. Flux decomposition

As emphasized by Hill [31], the kinetics of enzymatic networks for nonequilibrium steady states can be described in terms of probability fluxes assigned to directed cycles or dicycles of the network. At steady state, each cycle $\mathcal{C}_\nu$ carries two opposing dicycle fluxes $J(\mathcal{C}_\nu^d)$, which count the average number of times this cycle will be completed per second in a given direction, $d =$ "+" or $d =$ "−." These dicycle fluxes have the general form [5,31]

$$J(\mathcal{C}_\nu^d) = \Pi_\omega(\mathcal{C}_\nu^d)\frac{\Upsilon(\mathcal{C}_\nu)}{\Omega}, \qquad (3)$$

where

$$\Pi_\omega(\mathcal{C}_\nu^d) \equiv \prod_{|ij\rangle}^{\mathcal{C}_\nu^d} \omega_{ij} \qquad (4)$$

denotes the transition rate product along a directed cycle. In (3) the influent factor $\Upsilon(\mathcal{C}_\nu)$ represents a statistical weight of the cycle $\mathcal{C}_\nu$, which measures the flux onto the cycle from the rest of the network, while $\Omega$ is a normalization factor. Both terms consist of multilinear polynomials of the transition rates $\omega_{ij}$ and are strictly positive, although they depend on the control parameters [ATP], [ADP], [P], and $F$ in a nontrivial way. The dicycle excess fluxes in a given direction are defined by the difference

$$\Delta J(\mathcal{C}_\nu^+) = J(\mathcal{C}_\nu^+) - J(\mathcal{C}_\nu^-), \qquad (5)$$

with $\Delta J(\mathcal{C}_\nu^-) = -\Delta J(\mathcal{C}_\nu^+)$.[1] The local excess fluxes (1) can be decomposed into nonlocal dicycle excess fluxes via [5,31]

---

[1]The fluxes $\Delta J(\mathcal{C}_\nu^d)$ were previously denoted by $J(\mathcal{C}_\nu)$; see Eq. (8) of [5].
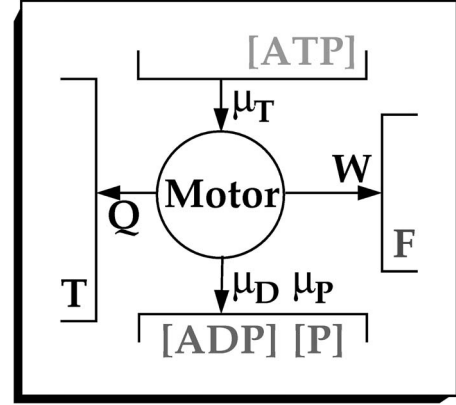


FIG. 3. Energy flux diagram for molecular motors driven by ATP hydrolysis. Binding of ATP to the motor implies an internal energy gain $\mu_T$, while the release of ADP and P changes the internal energy of the motor molecule by $-\mu_D$ and $-\mu_P$, respectively [30]. The chemical potential difference $\Delta\mu = \mu_T - \mu_D - \mu_P$ for the hydrolysis of one ATP molecule can be expressed in terms of the nucleotide concentrations, while the mechanical work per step, $W = \ell F$ as in (7), depends on the applied load force $F$ and on the mechanical step size $\ell$. The dissipated heat $Q$ then follows from the conservation of energy, as in (10).

$$\Delta J_{ij} = \sum_\nu \epsilon_{ij,\nu}\Delta J(\mathcal{C}_\nu^+), \qquad (6)$$

where $\epsilon_{ij,\nu} = \pm 1$, if the directed edge $|ij\rangle$ is an element of the directed cycle $\mathcal{C}_\nu^\pm$, and $\epsilon_{ij,\nu} = 0$, if the edge $\langle ij\rangle$ is not contained in the cycle $\mathcal{C}_\nu$. Thus, the sum in (6) includes all dicycle excess fluxes of the network that contribute to the transition $|ij\rangle$.

### B. Dicycle energy balance

As indicated in Fig. 3, the motor is in thermal equilibrium with a heat bath of temperature $T$. In the following, we consider room temperature with $T = 300$ K and define the rescaled load force and the rescaled chemical potential difference for the hydrolysis of one ATP molecule via

$$\bar{F} \equiv \frac{\ell F}{k_B T} = \frac{W}{k_B T}, \quad \Delta\bar{\mu} \equiv \frac{\Delta\mu}{k_B T} = \ln\left(\frac{K^{\text{eq}}[\text{ATP}]}{[\text{ADP}][\text{P}]}\right), \qquad (7)$$

with the Boltzmann constant $k_B$, the mechanical step size $\ell$, and the work $W$ performed by the motor during one mechanical step. In dilute solutions the potential difference $\Delta\mu = \mu_T - \mu_D - \mu_P$ can be expressed in terms of the concentrations for ATP, ADP, and P and the equilibrium constant for ATP hydrolysis $K^{\text{eq}}$ [30]. The value of the equilibrium constant

$$K^{\text{eq}} = [\text{ADP}][\text{P}]/[\text{ATP}]|^{\text{eq}} \simeq 4.9 \times 10^{11} \ \mu\text{M} \qquad (8)$$

is obtained from the ATP, ADP, and P concentrations in chemical equilibrium—i.e., when ATP hydrolysis and ATP synthesis balance [23,34].

Because $K^{\text{eq}}$ is large, the equilibrium of ATP hydrolysis corresponds to very small substrate concentrations [ATP] $\ll$ [ADP][P]. An increase of [ATP] for constant product con-

centrations induces excess hydrolysis. The catalytic action of the kinesin molecule channels the hydrolysis reaction pathway to extract mechanical work from the released chemical energy $\Delta\mu$; see Fig. 3. Since the motor operates isothermally, this energy transduction process also involves heat release.

Based on the dynamical properties of the steady state, we derived in [5,30] dicycle energy balance relations between the heat release for completing a cycle $\mathcal{C}_\nu^d$ in the state space network and the transition rates $\omega_{ij}$ of the dynamics. This energy balance links the product of transition rates of the cycle $\mathcal{C}_\nu^d$ to the corresponding numbers of hydrolyzed and synthesized ATP molecules and of forward and backward steps. If a catalytic cycle $\mathcal{C}_\nu^+$ involves the hydrolysis of $n_\mathrm{h}$ and the synthesis of $n_\mathrm{s}$ ATP molecules, as well as $m_\mathrm{f}$ forward and $m_\mathrm{b}$ backward mechanical steps each of size $\ell$, the dicycle balance relations have the general form [5,30]

$$\ln\frac{\Pi_\omega(\mathcal{C}_\nu^+)}{\Pi_\omega(\mathcal{C}_\nu^-)} = [n_\mathrm{h}(\mathcal{C}_\nu^+) - n_\mathrm{s}(\mathcal{C}_\nu^+)]\Delta\bar\mu - [m_\mathrm{f}(\mathcal{C}_\nu^+) - m_\mathrm{b}(\mathcal{C}_\nu^+)]\bar F \tag{9}$$

$$= \Delta\bar Q(\mathcal{C}_\nu^+), \tag{10}$$

where $\Delta\bar Q(\mathcal{C}_\nu^+)$ represents the heat released during completion of the dicycle $\mathcal{C}_\nu^+$ in units of $k_B T$. For the seven-state network in Fig. 2, the heat release of the six different cycles is given by

$$\Delta\bar Q(\mathcal{F}_1^+) = \Delta\bar Q(\mathcal{F}_2^+) = \Delta\bar\mu - \bar F, \tag{11}$$

$$\Delta\bar Q(\mathcal{B}^+) = \Delta\bar\mu + \bar F, \tag{12}$$

$$\Delta\bar Q(\mathcal{D}_1^+) = \Delta\bar Q(\mathcal{D}_2^+) = 2\Delta\bar\mu, \tag{13}$$

$$\Delta\bar Q(\mathcal{S}^+) = 0. \tag{14}$$

Comparing (10)–(14) with (2) and (7), one immediately gets for the transition rate constants the balance condition

$$\frac{\kappa_{12}\kappa_{25}\kappa_{56}\kappa_{61}}{\kappa_{21}\kappa_{52}\kappa_{65}\kappa_{16}} = \frac{\kappa_{12}\kappa_{25}\kappa_{57}\kappa_{71}}{\kappa_{21}\kappa_{52}\kappa_{75}\kappa_{17}} = \frac{\kappa_{45}\kappa_{52}\kappa_{23}\kappa_{34}}{\kappa_{54}\kappa_{25}\kappa_{32}\kappa_{43}} = K^\mathrm{eq}. \tag{15}$$

Furthermore, if one assumes that the internal energies of the motor states are independent of the load force, a local form of the balance conditions as derived in [30] implies that the load dependences of the stepping transition must fulfill the condition

$$\frac{\Phi_{25}(\bar F)}{\Phi_{52}(\bar F)} = e^{-\bar F}, \tag{16}$$

which is assured by the simple parametrization $\Phi_{25}(\bar F) = e^{-\theta\bar F}$ and $\Phi_{52}(\bar F) = e^{(1-\theta)\bar F}$ as used in [4]. The balance condition (9) also imposes constraints on the load dependences of the chemical transitions as given by

$$\frac{\Phi_{12}\Phi_{56}\Phi_{61}}{\Phi_{21}\Phi_{65}\Phi_{16}} = \frac{\Phi_{12}\Phi_{57}\Phi_{71}}{\Phi_{21}\Phi_{75}\Phi_{17}} = \frac{\Phi_{45}\Phi_{23}\Phi_{34}}{\Phi_{54}\Phi_{32}\Phi_{43}} = 1. \tag{17}$$

The local form of the balance condition leads to the stronger constraint [30]

$$\frac{\Phi_{ij}(\bar F)}{\Phi_{ji}(\bar F)} = 1 \quad \text{for } \langle ij\rangle \neq \langle 25\rangle, \tag{18}$$

which we have incorporated in [4] by the explicit form $\Phi_{ij} = 2/(1+e^{\chi_{ij}\bar F})$ with dimensionless coefficients $\chi_{ij} = \chi_{ji}$.

In general, the load-dependent factors $\Phi_{ij}(\bar F)$ must fulfill several general constraints which follow directly from the definition of $\Phi_{ij}(\bar F)$ in (2): (i) Since transition rates $\omega_{ij}$ cannot be negative, one has $\Phi_{ij}(\bar F) \geq 0$ for all load forces $\bar F$; (ii) likewise, transition rates cannot become arbitrarily large, which implies $\Phi_{ij}(\bar F) < \infty$ for all $\bar F$; and (iii) for vanishing load, $\Phi_{ij}(\bar F=0) = 1$ as in (2).

In addition, we have imposed the condition (iv) that the derivative $\partial\Phi_{ij}(\bar F)/\partial(\bar F)$ at $\bar F=0$ be consistent with the derivative of the motor velocity $v$ with respect to the load force $F$ as measured experimentally for small and large ATP concentrations. For small [ATP], the velocity $v$ is proportional to the transition rate $\omega_{12}$ since the rate limiting transition is provided by ATP binding. For large [ATP], on the other hand, the velocity is proportional to the transition rate product $\omega_{56}\omega_{61}$ since the ADP release transition $|56\rangle$ and the P release transition $|61\rangle$ are rate limiting in this case. Therefore, one has

$$\partial v/\partial F \propto \partial\Phi_{12}/\partial\bar F \quad \text{for small [ATP]} \tag{19}$$

and

$$\partial v/\partial F \propto \partial(\Phi_{56}\Phi_{61})/\partial\bar F \quad \text{for large [ATP]}. \tag{20}$$

Our parametrization $\Phi_{ij}(\bar F) = 2/(1+e^{\chi_{ij}\bar F})$ fulfills the three constraints (i)–(iii) and introduces only one additional parameter, namely $\chi_{ij}$. The latter parameter satisfies

$$\chi_{ij} = -2\partial\Phi_{ij}/\partial\bar F \quad \text{at } \bar F=0 \tag{21}$$

and, thus, can be directly determined, via (19) and (20), from the derivative $\partial v/\partial F$ at $F=0$ as measured experimentally. In order to go beyond our parametrization of $\Phi_{ij}(\bar F)$, one would need direct experimental information about the force dependence of the chemical transition rates. The latter information is, however, not available at present.

### C. Factorization of dicycle excess fluxes

Using the relations (9) and (10), one can factorize the dicycle excess fluxes as given by (5) in the form

$$\Delta J(\mathcal{C}_\nu^d) = (1 - e^{-\Delta\bar Q(\mathcal{C}_\nu^d)})\Pi_\omega(\mathcal{C}_\nu^d)\frac{\Upsilon(\mathcal{C}_\nu)}{\Omega}. \tag{22}$$

The first factor on the right-hand side of (22) accounts for the irreversibility of the pathway $\mathcal{C}_\nu^d$ and is entirely determined
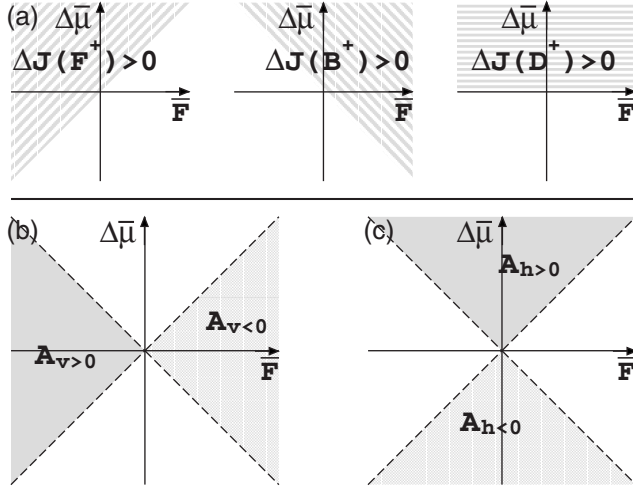
FIG. 4. (a) Sign of the dicycle excess fluxes $\Delta J(\mathcal{C}_\nu^+)$ as functions of the chemical potential difference $\Delta\bar\mu$ and the applied load $\bar F$. Gray dashed regions correspond to positive excess fluxes as in (26)–(28). (b) The regions in (a) determine two quarters $A_{v>0}$ and $A_{v<0}$ in the $(\Delta\bar\mu, \bar F)$ plane with positive and negative motor velocity $v$, respectively. The stall force, at which the velocity vanishes, defines a transition line that lies within the complementary, white regions and depends, in general, on the detailed kinetics of the different excess dicycle fluxes. (c) The signs of the dicycle excess fluxes in (a) also determine two regions of positive and negative ATP hydrolysis rate, $A_{h>0}$ and $A_{h<0}$, respectively. The line $h=0$ is located in the white regions.

by the energetics of this cycle; see, e.g., (11)–(14). Increasing the irreversibility of a closed pathway increases the excess probability flux on this cycle. In chemical and mechanical equilibrium with $\Delta\bar Q(\mathcal{C}_\nu^d)=0$, the dicycle excess flux $\Delta J(\mathcal{C}_\nu^d)$ vanishes, which is equivalent to full reversibility described by $J(\mathcal{C}_\nu^d)=J(\mathcal{C}_\nu^{-d})$. Far from equilibrium, on the other hand, the dicycle excess flux has the asymptotic behavior

$$\Delta J(\mathcal{C}_\nu^d) \approx J(\mathcal{C}_\nu^d) \quad \text{for large } \Delta\bar Q(\mathcal{C}_\nu^d). \tag{23}$$

The second factor $\Pi_\omega$ in (22) is a measure for the speed of a cycle completion in the direction of $\mathcal{C}_\nu^d$. Even cycles with a very large irreversibility may carry a small excess probability flux if the transitions in the corresponding direction are slow. Finally, the third factor $\Upsilon/\Omega$ is a topological term that describes the connection of the cycle $\mathcal{C}_\nu$ to the remaining network structure. Cycles that can be reached easily from the whole state space network obviously have larger probability fluxes than cycles that are only weakly connected to the rest of the network. In summary, the relevance of a closed pathway or cycle in a chemomechanical network is given by (i) its irreversibility, (ii) the speed in the direction determined by (i), and (iii) its connection to the rest of the state space network.

### D. Sign of dicycle excess fluxes

All factors in the expression (22) for the dicycle excess flux are strictly positive apart from the first one. This implies that the sign of the dicycle excess flux $\Delta J(\mathcal{C}_\nu^d)$ is equal to the

sign of the corresponding released heat $\Delta\bar Q(\mathcal{C}_\nu^d)$ or

$$\text{sgn}[\Delta J(\mathcal{C}_\nu^d)] = \text{sgn}[\Delta\bar Q(\mathcal{C}_\nu^d)], \tag{24}$$

$$\Delta J(\mathcal{C}_\nu^d) = 0 \quad \text{iff } \bar Q(\mathcal{C}_\nu^d) = 0. \tag{25}$$

For the seven-state model considered here, the heat release of the different cycles is given by (11)–(13). It then follows that the dicycle excess fluxes of the two forward-stepping dicycles satisfy

$$\Delta J(\mathcal{F}^+) > 0 \quad \text{for } \Delta\bar\mu > \bar F$$

$$= 0 \quad \text{for } \Delta\bar\mu = \bar F$$

$$< 0 \quad \text{for } \Delta\bar\mu < \bar F, \tag{26}$$

with $\Delta J(\mathcal{F}^+) \equiv \Delta J(\mathcal{F}_1^+) + \Delta J(\mathcal{F}_2^+)$. Note that the same relation holds for the sign of the individual dicycle fluxes—i.e., $\text{sgn}[\Delta J(\mathcal{F}_1^+)] = \text{sgn}[\Delta J(\mathcal{F}_2^+)] = \text{sgn}[\Delta J(\mathcal{F}^+)]$. In contrast, for the excess flux on the backward-stepping dicycle, one obtains

$$\Delta J(\mathcal{B}^+) > 0 \quad \text{for } \Delta\bar\mu > -\bar F$$

$$= 0 \quad \text{for } \Delta\bar\mu = -\bar F$$

$$< 0 \quad \text{for } \Delta\bar\mu < -\bar F. \tag{27}$$

Finally, the sign of the dissipative dicycle excess fluxes is determined by the chemical potential difference $\Delta\bar\mu$ alone and is given by

$$\Delta J(\mathcal{D}^+) > 0 \quad \text{for } \Delta\bar\mu > 0$$

$$= 0 \quad \text{for } \Delta\bar\mu = 0$$

$$< 0 \quad \text{for } \Delta\bar\mu < 0, \tag{28}$$

with $\Delta J(\mathcal{D}^+) \equiv \Delta J(\mathcal{D}_1^+) + \Delta J(\mathcal{D}_2^+)$ and $\text{sgn}[\Delta J(\mathcal{D}_1^+)] = \text{sgn}[\Delta J(\mathcal{D}_2^+)] = \text{sgn}[\Delta J(\mathcal{D}^+)]$. Relations (26)–(28) are illustrated in Fig. 4(a). Note that the factorization in (22) together with the energy balance in (14) immediately implies that the dicycle excess flux on the thermal cycle vanishes, $\Delta J(\mathcal{S}^+) = 0$.

## IV. MODES OF MOTOR OPERATION

### A. Motor velocity and ATP hydrolysis rate

The motor velocity $v$ is given by

$$v = \ell \Delta J_{25}, \tag{29}$$

i.e., by the step length $\ell$ times the excess probability flux $\Delta J_{25}$ along the stepping transition; see Fig. 2. It then follows from (6) that

$$v = \ell[\Delta J(\mathcal{F}_1^+) + \Delta J(\mathcal{F}_2^+) - \Delta J(\mathcal{B}^+)] \tag{30}$$

$$= \ell[\Delta J(\mathcal{F}^+) - \Delta J(\mathcal{B}^+)]. \tag{31}$$

Similarly, the ATP hydrolysis rate of the kinesin network model in Fig. 2 is given by

$$h = \Delta J_{61} + \Delta J_{57} + \Delta J_{34} \tag{32}$$

or

$$h = \Delta J(\mathcal{F}_1^+) + \Delta J(\mathcal{F}_2^+) + \Delta J(\mathcal{B}^+) + 2\Delta J(\mathcal{D}_1^+) + 2\Delta J(\mathcal{D}_2^+) \tag{33}$$

$$= \Delta J(\mathcal{F}^+) + \Delta J(\mathcal{B}^+) + 2\Delta J(\mathcal{D}^+), \tag{34}$$

According to (31), (34), and (5), the motor velocity and the hydrolysis rate depend on the dicycle excess fluxes and, thus, on the transition rates $\omega_{ij}$ of the network model. Furthermore, as stated in connection with (2), the transition rates depend on the control parameters provided by load force $F$ as well as substrate and product concentrations [ATP], [ADP], and [P]. The model parameters are the transition rate constants $\kappa_{ij}$ and the $F$-dependent factors $\Phi_{ij}$.

Comparing the motor velocity with single-molecule data on processively moving kinesin motors as obtained in [22–25], we could determine the model parameters for the forward-stepping cycles [4,37]. In the absence of any experimental data about the rates of the backward-stepping cycle $\mathcal{B}$, the simplest assumption about the transition rates of this cycle is to choose these rates to be identical with the corresponding ones of the forward-stepping cycle $\mathcal{F}_1$ apart from one such rate which was taken to be $\omega_{54}$ in [4] as reviewed in Appendix A 2.

### B. Sign of motor velocity and stall force

When expression (31) for the motor velocity is combined with the two relations (26) and (27) for the sign of the two dicycle excess fluxes $\Delta J(\mathcal{F}^+)$ and $\Delta J(\mathcal{B}^+)$, one concludes that $v$ is positive in region $A_{v>0}$ and negative in region $A_{v<0}$ where these two regions represent tilted quarters of the $(\bar{F}, \Delta\bar{\mu})$ plane as defined by

$$A_{v>0} \equiv \{\bar{F} < 0, \bar{F} \leqslant \Delta\bar{\mu} \leqslant -\bar{F}\},$$

$$A_{v<0} \equiv \{\bar{F} > 0, -\bar{F} \leqslant \Delta\bar{\mu} \leqslant \bar{F}\}. \tag{35}$$

These two quarters lie opposite to each other and are separated by the two complementary quarters of this plane; see Fig. 4(b). Note that the two regions $A_{v>0}$ and $A_{v<0}$ include their boundary lines with $\Delta\bar{\mu} = \bar{F} \neq 0$ and $\Delta\bar{\mu} = -\bar{F} \neq 0$ and, thus, are closed subsets of the $(\bar{F}, \Delta\bar{\mu})$ plane apart from the origin $(\bar{F}, \Delta\bar{\mu}) = (0, 0)$.

It now follows from (35) that the zeros of the motor velocity must lie in the two complementary quarters which represent open subsets of the $(\bar{F}, \Delta\bar{\mu})$ plane corresponding to the unshaded areas in Fig. 4(b). For given substrate and product concentrations [ATP], [ADP], and [P], the zeros of the velocity determine the stall force of the motor—i.e.,

$$v(\bar{F}, [\text{ATP}], [\text{ADP}], [\text{P}]) = 0 \quad \text{for } \bar{F} = \bar{F}_{\text{s}}. \tag{36}$$

In the following, we will study the stall force equation (36) for the seven-state network model as shown in Fig. 2. Since the motor velocity $v$ is proportional to the excess flux $\Delta J_{25}$ as in (29), this stall force equation is equivalent to mechanical equilibrium between the motor states $i = 2$ and $i = 5$. Using the decomposition (30), the velocity will be expressed in terms of dicycle excess fluxes, which depend on all transition rates $\omega_{ij}$ including the rates for the binding of ATP, ADP, and P, which are proportional to [ATP], [ADP], and [P]. It will then become apparent that the stall force $\bar{F}_{\text{s}}$ depends, in general, on all three concentrations [ATP], [ADP], and [P]. However, we will also show that one can define a small concentration limit in which the stall force becomes a function of the chemical potential difference $\Delta\bar{\mu}$ only.

In terms of dicycle excess fluxes, the stall condition reads $\Delta J(\mathcal{F}^+) = \Delta J(\mathcal{B}^+)$, which implies, using (11), (12), and (22),

$$\frac{1 - e^{-\Delta\bar{\mu} - \bar{F}}}{1 - e^{-\Delta\bar{\mu} + \bar{F}}} Z_1 = 1 + Z_2 \quad \text{for } \bar{F} = \bar{F}_{\text{s}} \tag{37}$$

[see (A6) and (A8)], with

$$Z_1 \equiv \frac{\Pi_\omega(\mathcal{B}^+)}{\Pi_\omega(\mathcal{F}_1^+)} \frac{Y(\mathcal{B})}{Y(\mathcal{F}_1)} \tag{38}$$

and

$$Z_2 \equiv \frac{\Pi_\omega(\mathcal{F}_2^+)}{\Pi_\omega(\mathcal{F}_1^+)} \frac{Y(\mathcal{F}_2)}{Y(\mathcal{F}_1)}. \tag{39}$$

For both $Z_1$ and $Z_2$, the first fraction involving the transition rate products $\Pi_\omega$ does not depend on any concentration, whereas the second fraction involving the influent factors $Y$ depends on all three concentrations [ADP], [P], and [ATP] $\sim \exp(-\Delta\bar{\mu})$ as follows from the explicit expressions for these latter factors as given by (A2).

In the limit of vanishing product concentrations [ADP] = [P] = 0, the chemical potential difference $\Delta\bar{\mu}$ as given by (7) diverges and the stall force relation (37) reduces to the simple expression

$$\frac{\omega_{52}\omega_{23}}{\omega_{25}\omega_{56}} = 1 + \frac{\omega_{57}}{\omega_{56}} \quad \text{for } \bar{F} = \bar{F}_\infty, \tag{40}$$

which defines the limiting stall force $\bar{F}_{\text{s}} = \bar{F}_\infty$. For the "symmetric" model, which implies (A14) and the equality $\omega_{23} = \omega_{56}$ for the ADP release transition rates of the trailing and leading heads, relations (16) and (40) lead to

$$\frac{\kappa_{25}}{\kappa_{52}} = \frac{e^{\bar{F}_\infty}}{1 + \omega_{57}/\omega_{56}|_{\bar{F}_\infty}}, \tag{41}$$

where (16) has been used. The ratio $\omega_{57}/\omega_{56}$ measures the competition between the two alternative pathways of (i) ATP hydrolysis at the trailing head during the transition $|57\rangle$ followed by ADP release at the leading head and (ii) ADP release at the leading head during the transition $|56\rangle$ and subsequent cleavage of the bound ATP at the trailing head;

compare Fig. 2. Since the load dependences of the ADP release transition $|56\rangle$ and the hydrolysis transition $|57\rangle$ are not known, we make the simplifying assumption $\Phi_{56}=\Phi_{57}$, which cancels the load dependence and leads to $\omega_{57}/\omega_{56}=\kappa_{57}/\kappa_{56}$. This implies the limiting stall force

$$\bar{F}_\infty = \ln\left[\frac{\kappa_{25}}{\kappa_{52}}\left(1+\frac{\kappa_{57}}{\kappa_{56}}\right)\right]. \qquad (42)$$

Comparison of the model dynamics with the observed behavior of the kinesin motor velocity then leads to $\kappa_{57}/\kappa_{56} \simeq 0.5$ [4,37]. With the mechanical step size $\ell \simeq 8$ nm [14,15], stall force $F_\infty \simeq 7$ pN [22,24], and thermal energy $k_BT \simeq 4$ pN nm (room temperature), we find from (41) that the ratio $\kappa_{25}/\kappa_{52} \propto e^{14} \sim 10^6 \gg 1$.

For the symmetric model as defined by (A4) and (A5), the implicit equation (37) for the stall force simplifies, since the terms $Z_1$ and $Z_2$ then have the explicit form

$$Z_1 = \frac{\omega_{52}}{\omega_{25}}\left(1+\frac{(\omega_{61}+\omega_{65})\omega_{17}\omega_{75}}{(\omega_{71}+\omega_{75})(\omega_{12}\omega_{65}+\omega_{12}\omega_{61}+\omega_{16}\omega_{65})}\right) \qquad (43)$$

and

$$Z_2 = \frac{(\omega_{61}+\omega_{65})\omega_{57}\omega_{71}}{(\omega_{71}+\omega_{75})\omega_{56}\omega_{61}}; \qquad (44)$$

see (A10) and (A11).

We now define the one-dimensional concentration coordinate $K$ via

$$K \equiv \frac{[\text{ADP}][\text{P}]}{[\text{ATP}]}, \qquad (45)$$

which implies

$$e^{-\Delta\bar{\mu}} = \frac{K}{K^{\text{eq}}}, \qquad (46)$$

and consider the limit in which all three concentrations [ATP], [ADP], and [P] become small, but with constant parameter $K$ and, thus, constant $\Delta\bar{\mu}$. In this limit, the stall force condition (37) becomes

$$\frac{1-e^{-\Delta\bar{\mu}-\bar{F}_s}}{1-e^{-\Delta\bar{\mu}+\bar{F}_s}}e^{\bar{F}_s-\bar{F}_\infty} \approx 1, \qquad (47)$$

with the explicit solution

$$\bar{F}_s \approx \ln\left(\frac{e^{\bar{F}_\infty}+e^{-\Delta\bar{\mu}}}{e^{\bar{F}_\infty-\Delta\bar{\mu}}+1}\right) \equiv \bar{F}_s(\Delta\bar{\mu}). \qquad (48)$$

Thus, in this small-concentration limit with fixed chemical potential difference $\Delta\bar{\mu}$, the stall force $\bar{F}_s$ depends only on this chemical potential difference and no longer on the three activities or concentrations separately. Expression (48) has the asymptotic behavior

$$\bar{F}_s \approx \bar{F}_\infty \quad \text{for large } \Delta\bar{\mu} \qquad (49)$$

and
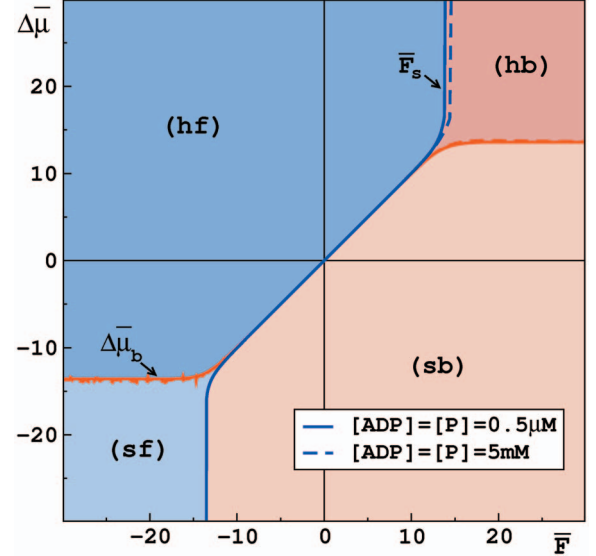


FIG. 5. (Color) Operation diagram for kinesin: the $(\bar{F},\Delta\bar{\mu})$ plane is divided up into four different regions denoted by (hf), (hb), (sb), and (sf) corresponding to four different operation modes of the motor. The regions (hf) and (hb) represent ATP hydrolysis coupled to forward and backward stepping, whereas the regions (sb) and (sf) correspond to ATP synthesis coupled to backward and forward stepping. The boundaries between these four regions are provided by the stall force lines (blue) as given by $\bar{F}_s=\bar{F}_s(\Delta\bar{\mu})$ and by the balanced potential lines (red) as described by $\Delta\bar{\mu}_b=\Delta\bar{\mu}_b(\bar{F})$. The solid and dashed lines have been obtained by solving the implicit equations (37) and (53) with (43), (44), and (56) numerically for product concentrations [ADP]=[P]=0.5 $\mu$M and 5 mM, respectively. In addition, expressions (48) and (58) have also been plotted, but the resulting lines are indistinguishable from the solid lines as obtained via the numerical solution.

$$\bar{F}_s \approx \frac{e^{\bar{F}_\infty}-1}{e^{\bar{F}_\infty}+1}\Delta\bar{\mu} \quad \text{for small } \Delta\bar{\mu}. \qquad (50)$$

In Fig. 5, we have plotted the stall force $\bar{F}_s$ as a function of $\Delta\bar{\mu}$ for the product concentrations [ADP]=[P]=0.5 $\mu$M and [ADP]=[P]=5 mM as obtained by solving the implicit equation (37) for the symmetric model with (43) and (44) numerically. In addition, we also plotted expression (48) for the stall force as obtained in the small-concentration limit with constant $\Delta\bar{\mu}$. In Fig. 5, the stall force obtained from (48) is indistinguishable from the numerical solution of (37) for [ADP]=[P]=0.5 $\mu$M and provides a rather good approximation to the numerical solution even for [ADP]=[P] =5 mM.

### C. Sign of hydrolysis rate and balanced potential

Using the same line of reasoning as in the previous subsection, we find from the general expression (34) for the hydrolysis rate $h$ together with the inequalities (26)–(28) for the dicycle excess fluxes that $h$ is positive in $A_{h>0}$ and negative in $A_{h<0}$, where these two regions also represent tilted quarters of the $(\bar{F},\Delta\bar{\mu})$ plane as defined by

$$A_{h>0} \equiv \{\Delta\bar{\mu} > 0, -\Delta\bar{\mu} \le \bar{F} \le \Delta\bar{\mu}\},$$

$$A_{h<0} \equiv \{\Delta\bar{\mu} < 0, \Delta\bar{\mu} \le \bar{F} \le -\Delta\bar{\mu}\}; \quad (51)$$

see Fig. 4(c). It follows from (51) that the zeros of the hydrolysis rate $h$ must lie within the white regions in Fig. 4(c), which are complementary to both $A_{h>0}$ and $A_{h<0}$.

Just as the zeros of the motor velocity define the stall force, the zeros of the hydrolysis rate $h$ define the balanced activities or concentrations of the motor—i.e.,

$$h(\bar{F}, [\text{ATP}], [\text{ADP}], [\text{P}]) = 0. \quad (52)$$

More precisely, this relation defines, for fixed load force $\bar{F}$, a two-dimensional subspace in the three-dimensional activity space spanned by [ATP], [ADP], and [P], and one may then express one activity as a function of the two other activities and of the load force. Furthermore, using the definition (7) of the chemical potential difference $\Delta\bar{\mu}$, one may express the concentration [ATP] in terms of $\Delta\bar{\mu}$, [ADP], and [P]. The solution of (52) then leads to a balanced potential $\Delta\bar{\mu}_b$ that depends on the load force $\bar{F}$ as well as on the two product concentrations [ADP] and [P].

In the following, we will study relation (52) for the seven-state network model as shown in Fig. 2. Using the decomposition (33), the hydrolysis rate will be expressed in terms of dicycle excess fluxes, which again depend on all three activities or concentrations [ATP], [ADP], and [P]. As in the case of the stall force, we will also consider the small-concentration limit with fixed chemical potential difference $\Delta\bar{\mu}$, which leads to a balanced potential $\Delta\bar{\mu}_b$ that depends only on the load force $\bar{F}$.

When the hydrolysis rate $h$ is expressed in terms of the dicycle excess fluxes via (33), the balanced activities are determined by the condition $\Delta J(\mathcal{F}^+) + \Delta J(\mathcal{B}^+) + 2\Delta J(\mathcal{D}^+) = 0$, which is equivalent to

$$\frac{1 - e^{-\Delta\bar{\mu} - \bar{F}_s}}{1 - e^{-\Delta\bar{\mu} + \bar{F}_s}} Z_1 = -(1 + Z_2) \times \left(1 + 2\frac{1 - e^{-2\Delta\bar{\mu}}}{1 - e^{-\Delta\bar{\mu} + \bar{F}}} Z_3\right) \quad (53)$$

[compare (A6)–(A9)], with $Z_1$ and $Z_2$ as defined by (38) and (39) and the additional term

$$Z_3 \equiv \frac{\Pi_\omega(\mathcal{D}_1^+)}{\Pi_\omega(\mathcal{F}_1^+)} \frac{Y(\mathcal{D}_1)}{Y(\mathcal{F}_1)}. \quad (54)$$

In order to derive relation (53), we also used the fact that the term $Z_2$ as defined by (39) satisfies the additional equality

$$Z_2 = \frac{\Pi_\omega(\mathcal{D}_2^+) Y(\mathcal{D}_2)}{\Pi_\omega(\mathcal{D}_1^+) Y(\mathcal{D}_1)}. \quad (55)$$

For the symmetric model as defined in Appendix A 2, the term $Z_3$ as given by (54) has the explicit form

$$Z_3 = \frac{\omega_{12}\omega_{56}\omega_{61}}{\omega_{25}(\omega_{12}\omega_{65} + \omega_{12}\omega_{61} + \omega_{16}\omega_{65})} \quad (56)$$

in terms of the transition rates $\omega_{ij}$. Performing now the limit of small concentrations for ATP, ADP, and P for fixed chemical potential difference as introduced in (45) and (46), the transition rate polynomials in (43), (44), and (56) simplify and lead to the condition

$$\frac{1 - e^{-\Delta\bar{\mu}_b - \bar{F}}}{1 - e^{-\Delta\bar{\mu}_b + \bar{F}}} e^{\bar{F} - \bar{F}_\infty} \approx -\left(1 + 2\frac{\omega_{23}}{\omega_{25}}\frac{1 - e^{-2\Delta\bar{\mu}_b}}{1 - e^{-\Delta\bar{\mu}_b + \bar{F}}}\right) \quad (57)$$

for the balanced activities where relations (A13)–(A15) have been used.

The transition rate ratio $\omega_{23}/\omega_{25}$ depends explicitly on the load force $\bar{F}$ and measures the competition between (i) forward movement of the ADP containing and loosely bound trailing head towards the next binding site via the transition $|25\rangle$ and (ii) ADP release from the trailing head and subsequent tight binding of this head via $|23\rangle$; see Fig. 2. Thus, the motor is more likely to undergo the futile hydrolysis cycles $\mathcal{D}_1^+$ and $\mathcal{D}_2^+$ for larger values of $\omega_{23}/\omega_{25}$. However, for the transition rates as obtained from the experimental data, we found that the ratio $\omega_{23}/\omega_{25} \ll 1$ for the relevant range of load forces [4,37]; i.e., futile hydrolysis is strongly suppressed. Neglecting the term proportional to $\omega_{23}/\omega_{25}$ in (57), we obtain the explicit expression

$$\Delta\bar{\mu}_b \approx \ln\left(\frac{e^{\bar{F}_\infty} + e^{-\bar{F}}}{e^{\bar{F}_\infty - \bar{F}} + 1}\right) \equiv \Delta\bar{\mu}_b(\bar{F}) \quad (58)$$

for the balanced potential $\Delta\bar{\mu}_b$ with the limiting stall force $\bar{F}_\infty$ as given by (42). Expression (58) has the asymptotic behavior

$$\Delta\bar{\mu}_b \approx \Delta\bar{\mu}_\infty = \bar{F}_\infty \quad \text{for large } \bar{F} \quad (59)$$

and

$$\Delta\bar{\mu}_b \approx \frac{e^{\bar{F}_\infty} - 1}{e^{\bar{F}_\infty} + 1}\bar{F} \quad \text{for small } \bar{F}. \quad (60)$$

Thus, in the small-concentration limit with fixed $\Delta\bar{\mu}$, the hydrolysis rate $h$ vanishes for the balanced potential $\Delta\bar{\mu}_b$ as given by (58), which depends only on the load force $\bar{F}$.

In general, the balanced potential $\Delta\bar{\mu}_b$ follows from the implicit equation (52) or (53) for the balanced activities as mentioned previously. When [ATP] is expressed in terms of $\Delta\bar{\mu}$, [ADP], and [P], the general solution of (52) or (53) leads to a balanced potential $\Delta\bar{\mu}_b$ that depends on the load force $\bar{F}$ as well as on the two product concentrations [ADP] and [P].

In Fig. 5, we have plotted the balanced potential $\Delta\bar{\mu}_b$ as a function of $\bar{F}$ for the product concentrations [ADP]=[P] $= 0.5\ \mu$M and [ADP]=[P]=5 mM as obtained by a numerical solution of the implicit equation (53) for the symmetric model with (43), (44), and (56). In addition, we also plotted expression (58) for the balanced potential as obtained in the small-concentration limit with constant $\Delta\bar{\mu}$. Inspection of

Fig. 5 shows that the balanced potential as obtained from (58) is indistinguishable from the numerical solution of (53) for $[ADP]=[P]=0.5~\mu M$ and provides a rather good approximation to the numerical solution even for $[ADP]=[P]=5$ mM.

### D. Operation diagram

As shown in Fig. 5, the conditions of vanishing motor velocity and vanishing hydrolysis rate as discussed in the previous subsections divide the thermodynamic $(\bar{F}, \Delta\bar{\mu})$ plane into four different regions denoted by (hf), (hb), (sb), and (sf). These regions correspond to different operation modes of the motor: (i) In operation mode (hf), the motor couples ATP hydrolysis to forward mechanical steps. Depending on the ADP concentration, this mode is governed by the chemomechanical dicycles $\mathcal{F}_1^+$ and/or $\mathcal{F}_2^+$—i.e., by the chemomechanical cycles $\mathcal{F}_1$ and $\mathcal{F}_2$, which the motor traverses in the $d=+$ direction. (ii) In mode (hb), ATP hydrolysis is coupled to backward mechanical steps. This mode is dominated by the chemomechanical dicycle $\mathcal{B}^+$. (iii) In the operation mode (sb), the motor couples ATP synthesis to backward steps and is then governed by the chemomechanical dicycles $\mathcal{F}_1^-$ and/or $\mathcal{F}_2^-$. (iv) In the mode (sf), ATP synthesis is coupled to forward steps since the motor follows primarily the dicycle $\mathcal{B}^-$—i.e., the chemomechanical cycle $\mathcal{B}$ in the $d=-$ direction.

The boundaries between these four operation regions or modes are provided by (i) the stall force $\bar{F}_s$ as a function of the chemical potential difference $\Delta\bar{\mu}$ and (ii) the balanced potential $\Delta\bar{\mu}_b$ as a function of the load force $\bar{F}$, where both functions can be obtained, in general, for fixed product concentrations $[ADP]$ and $[P]$. In addition, we have defined a small concentration limit with constant $\Delta\bar{\mu}$, which leads to the explicit expressions (48) and (58) for these two functions. In Fig. 5, the functions $\bar{F}_s = \bar{F}_s(\Delta\bar{\mu})$ and $\Delta\bar{\mu}_b = \Delta\bar{\mu}_b(\bar{F})$ are shown as blue and red lines, respectively.

In the framework of ratchet models, an operation diagram with four different modes has also been obtained recently from a model that describes the interplay between a stepping pathway coupled to ATP hydrolysis and a diffusive stepping pathway. Compared to our diagram, the boundaries of these regions are, however, quite different. In particular, the operation diagram obtained in [35] exhibits no symmetry with respect to the line $\Delta\bar{\mu}=-\bar{F}$ and the region "sf" extends close to the line $\bar{F}=0$.

At mechanical and chemical equilibrium $\bar{F}=\Delta\bar{\mu}=0$, the two functions $\bar{F}_s(\Delta\bar{\mu})$ and $\Delta\bar{\mu}_b(\bar{F})$ intersect. Close to this chemomechanical equilibrium point, the stall force $\bar{F}_s = \bar{F}_s(\Delta\bar{\mu})$ and the balancing potential $\Delta\bar{\mu}_b = \Delta\bar{\mu}_b(\bar{F})$ approach the straight line $\bar{F}=\Delta\bar{\mu}$ as obtained from linear response theory [36]. Far from equilibrium, both functions saturate and attain constant values as given by $\bar{F}_\infty = \Delta\bar{\mu}_\infty \simeq 14$, [22,24,25].

For $\bar{F}_s \geq 0$, the reduced stall force $\bar{F}_s = \ell F_s / k_B T$ can be interpreted as a measure for the maximal work that the motor can perform during one mechanical step against an external load, while $\Delta\bar{\mu}$ represents the maximal amount of chemical energy the motor may use per hydrolyzed ATP molecule; see (7). Starting from chemical equilibrium $\Delta\bar{\mu}=0$ an initial increase in the chemical energy supply leads to a linear increase of the maximal work per step and $\bar{F}_s \propto \Delta\bar{\mu}$ with a proportionality coefficient that is very close to 1; see (50). A further increase of the supplied chemical energy brings the motor far away from equilibrium and leads to a saturation of the maximal work as estimated by $\bar{F}=\bar{F}_\infty$.

### V. SUMMARY

We have continued to study the seven-state network for the molecular motor kinesin (see Fig. 2), which we introduced in [4]. As shown in our previous work, this network provides a unified description for all experimental observations on the processive motion of kinesin. In contrast to conventional unicycle models, the seven-state network involves alternative and competing chemomechanical pathways or motor cycles. As shown in the present article, this network description also leads to four different operation modes of the motor as summarized in the operation diagram of Fig. 5. These four modes correspond to forward and backward mechanical steps coupled to ATP hydrolysis and synthesis. Mechanical slip cycles as discussed in [35] that lead to mechanical steps without ATP hydrolysis (or synthesis) are not considered here.

The different chemomechanical pathways contribute to the observable motor dynamics with different statistical weights, which depend on the external control parameters provided by the applied load force $F$ and the concentrations $[ATP]$, $[ADP]$, and $[P]$. The latter quantities define the chemical potential difference $\Delta\mu$, which together with the applied load $F$ determines the thermodynamic state of the motor. The $(\bar{F}, \Delta\bar{\mu})$ plane is divided into four regions corresponding to the four operation modes; see Fig. 5. The boundaries between the four operation modes are obtained from the implicit equations (36) and (37) for the stall force $\bar{F}_s$ and from the implicit equations (52) and (53) for the balanced potential $\Delta\bar{\mu}_b$. In general, these boundaries in the $(\bar{F}, \Delta\bar{\mu})$ plane depend on the product concentrations $[ADP]$ and $[P]$. In the small-concentration limit in which the concentration coordinate $K$ as defined in (45) remains constant, the boundaries can be described by functions $\bar{F}_s = \bar{F}_s(\Delta\bar{\mu})$ and $\Delta\bar{\mu}_b = \Delta\bar{\mu}_b(\bar{F})$ for which we have obtained the analytic expressions (48) and (58). These latter expressions also apply to small product concentrations $[ADP]$ and $[P]$ as illustrated in the operation diagram of Fig. 5 for $[ADP]=[P]=0.5~\mu M$. In fact, the dependence of the stall force $\bar{F}_s$ and the balanced potential $\Delta\bar{\mu}_b$ on the product concentrations $[ADP]$ and $[P]$ turns out to be rather weak over the entire range of experimentally relevant scales: Increasing the product concentrations from $[ADP]=[P]=0.5~\mu M$ to $[ADP]=[P]=5$ mM leads only to a slightly larger value for the stall force; see Fig. 5.

Our study shows that one has to distinguish mechanical equilibrium of a molecular motor, which occurs along the

stall force line $\bar{F}_s = \bar{F}_s(\Delta\bar{\mu})$, from its chemical equilibrium, which occurs along the balanced potential line $\Delta\bar{\mu}_b = \Delta\bar{\mu}_b(\bar{F})$. In the thermodynamic parameter space spanned by $\bar{F}$ and $\Delta\bar{\mu}$, chemomechanical equilibrium is only present at the origin $\bar{F} = \Delta\bar{\mu} = 0$.

Close to chemical equilibrium, the stall force $F_s$ increases linearly with the chemical potential difference $\Delta\mu$ as described by (50). Far away from chemical equilibrium—i.e., for large chemical potential differences—the reduced stall force attains the constant value $\bar{F}_s = \bar{F}_\infty \simeq 14$ as given by (42), which corresponds to $F_s = F_\infty \simeq 7$ pN. An energy supply of $\Delta\bar{\mu} > 14$ or $\Delta\mu > 14 k_B T$ does not increase the strength of the motor in terms of its stall force, but may lead to a higher motor velocity with the cost of additional heat dissipation.

In our model, the balanced potential $\Delta\bar{\mu}_b$ also saturates far from mechanical equilibrium—i.e., for large applied load forces $\bar{F}$. As a consequence, ATP synthesis against a positive chemical potential difference $\Delta\mu$ can only be induced by pulling the kinesin motor into the backward direction if $\Delta\mu$ does not exceed the limiting value $\Delta\bar{\mu}_\infty = \bar{F}_\infty$ as given by (59), which corresponds to $\Delta\mu_\infty \simeq 14 k_B T$ in physical units.

So far, two regimes of the operation diagram have been explored experimentally. First, most experimental studies in motility assays were performed for high ATP concentrations and relatively low ADP and P concentrations, which implies $\Delta\mu > \Delta\mu_\infty$. In this regime, increasing the load force $F$ leads to a transition from the (hf) mode to the (hb) mode—i.e., from forward steps coupled to ATP hydrolysis to backward steps again coupled to ATP hydrolysis. Second, Hackney [28] studied ATP synthesis by kinesin motors using high ADP and P concentrations and relatively low ATP concentrations, which implies $\Delta\mu < 0$. In these latter experiments the influence of an applied load has not been investigated. Our operation diagram in Fig. 5 predicts that the kinesin motor exhibits four operation modes and transitions between these modes. In particular, it is predicted that the motor undergoes a transition from the (hf) mode to the (sb) mode for small positive $\Delta\mu$ and increasing load; see Fig. 5. This transition as well as all other transitions in the operation diagram of Fig. 5 should be accessible to single-molecule experiments in which one varies both the load force $F$ and the chemical potential difference $\Delta\mu$ by controlling all three concentrations [ATP], [ADP], and [P] simultaneously.

## APPENDIX A: DETAILED DESCRIPTION OF THE SEVEN-STATE NETWORK FOR KINESIN

### 1. Transition rate polynomials determining the dicycle excess fluxes

In this subsection, we will provide explicit expressions for the different factors that enter the dicycle excess fluxes as given by (22). First, the products $\Pi_\omega$ of transition rates along the different dicycles of the seven-state network in Fig. 2 have the explicit form

$$\Pi_\omega(\mathcal{F}_1^+) = \omega_{12}\omega_{25}\omega_{56}\omega_{61},$$

$$\Pi_\omega(\mathcal{F}_2^+) = \omega_{12}\omega_{25}\omega_{57}\omega_{71},$$

$$\Pi_\omega(\mathcal{B}^+) = \omega_{45}\omega_{52}\omega_{23}\omega_{34},$$

$$\Pi_\omega(\mathcal{D}_1^+) = \omega_{12}\omega_{23}\omega_{34}\omega_{45}\omega_{56}\omega_{61},$$

$$\Pi_\omega(\mathcal{D}_2^+) = \omega_{12}\omega_{23}\omega_{34}\omega_{45}\omega_{57}\omega_{71}. \tag{A1}$$

Second, the influent factors $\Upsilon$ of the dicycles are given by

$$\Upsilon(\mathcal{F}_1) = (\omega_{71} + \omega_{75})(\omega_{32}\omega_{45} + \omega_{32}\omega_{43} + \omega_{34}\omega_{45}),$$

$$\Upsilon(\mathcal{F}_2) = (\omega_{61} + \omega_{65})(\omega_{32}\omega_{45} + \omega_{32}\omega_{43} + \omega_{34}\omega_{45}),$$

$$\Upsilon(\mathcal{B}) = (\omega_{71} + \omega_{75})(\omega_{12}\omega_{65} + \omega_{12}\omega_{61} + \omega_{16}\omega_{65}) + (\omega_{61}$$
$$+ \omega_{65})\omega_{17}\omega_{75},$$

$$\Upsilon(\mathcal{D}_1) = \omega_{71} + \omega_{75},$$

$$\Upsilon(\mathcal{D}_2) = \omega_{61} + \omega_{65}. \tag{A2}$$

For small [ADP] and [P], expressions (A2) simplify and become

$$\Upsilon(\mathcal{F}_1) \approx \omega_{71}\omega_{34}\omega_{45},$$

$$\Upsilon(\mathcal{F}_1) \approx \omega_{61}\omega_{34}\omega_{45},$$

$$\Upsilon(\mathcal{B}) \approx \omega_{71}\omega_{12}\omega_{61},$$

$$\Upsilon(\mathcal{D}_1) \approx \omega_{71},$$

$$\Upsilon(\mathcal{D}_2) \approx \omega_{61}. \tag{A3}$$

### 2. Symmetric forward- and backward-stepping model

By comparing the model dynamics of the seven-state network representation with observed properties of the processive kinesin walk from Refs. [22–27], we could only identify the rates of the forward-stepping cycles uniquely [4,37], because experiments addressed mainly this highly processive mode of operation for the kinesin motor. We therefore identified the rate constants of the chemical transitions on the cycle $\mathcal{B}$ with the corresponding ones on $\mathcal{F}_1$. The difference between these transitions are the relative positions of the two kinesin heads. For example, the transitions $|12\rangle$ and $|45\rangle$ describe ATP binding on the leading and trailing heads, respectively, whereas the other head contains ADP. However, because of thermodynamic constraints leading to (15), this identification is not possible for all transitions. As a consequence, we used

$$\kappa_{23} = \kappa_{56}, \quad \kappa_{32} = \kappa_{65},$$

$$\kappa_{34} = \kappa_{61}, \quad \kappa_{43} = \kappa_{16},$$

$$\kappa_{45} = \kappa_{12}, \quad \kappa_{54} = \kappa_{21}(\kappa_{52}/\kappa_{25})^2. \tag{A4}$$

In addition, we also assume the same load dependences for the chemical transitions of the leading and trailing heads, which implies

$$\Phi_{23}(F) = \Phi_{56}(F) = \Phi_{71}(F),$$

$$\Phi_{34}(F) = \Phi_{61}(F) = \Phi_{57}(F),$$

$$\Phi_{45}(F) = \Phi_{12}(F). \tag{A5}$$

### 3. Dicycle flux ratios

In the derivation of the implicit equations (37) and (53) for the stall force $\bar{F}_s$ and the balanced potential $\Delta\bar{\mu}_b$, one encounters ratios of different dicycle excess fluxes, which will be discussed in this subsection. It follows from the general form of the dicycle excess fluxes as given by (22) that the ratios of these fluxes lead, in general, to a product of three fractions, that involve the irreversibility factors $1 - e^{-\Delta\bar{Q}}$, the transition rate products $\Pi_\omega$, and the influent factors $\Upsilon$. For the chemomechanical cycles and the dissipative slip cycles, one finds

$$\frac{\Delta J(\mathcal{F}_2^+)}{\Delta J(\mathcal{F}_1^+)} = \frac{\Pi_\omega(\mathcal{F}_2^+)\Upsilon(\mathcal{F}_2)}{\Pi_\omega(\mathcal{F}_1^+)\Upsilon(\mathcal{F}_1)}, \tag{A6}$$

$$\frac{\Delta J(\mathcal{D}_2^+)}{\Delta J(\mathcal{D}_1^+)} = \frac{\Pi_\omega(\mathcal{D}_2^+)\Upsilon(\mathcal{D}_2)}{\Pi_\omega(\mathcal{D}_1^+)\Upsilon(\mathcal{D}_1)}, \tag{A7}$$

$$\frac{\Delta J(\mathcal{B}^+)}{\Delta J(\mathcal{F}_1^+)} = \frac{(1 - e^{-\Delta\bar{\mu} - \bar{F}})}{(1 - e^{-\Delta\bar{\mu} + \bar{F}})} \frac{\Pi_\omega(\mathcal{B}^+)\Upsilon(\mathcal{B})}{\Pi_\omega(\mathcal{F}_1^+)\Upsilon(\mathcal{F}_1)}, \tag{A8}$$

$$\frac{\Delta J(\mathcal{D}_1^+)}{\Delta J(\mathcal{F}_1^+)} = \frac{(1 - e^{-2\Delta\bar{\mu}})}{(1 - e^{-\Delta\bar{\mu} + \bar{F}})} \frac{\Pi_\omega(\mathcal{D}_1^+)\Upsilon(\mathcal{D}_1)}{\Pi_\omega(\mathcal{F}_1^+)\Upsilon(\mathcal{F}_1)}. \tag{A9}$$

From (A1) and (A2) it follows directly that the flux ratios (A6) and (A7) for the two alternative forward stepping di-

cycles $\mathcal{F}_1^+$ and $\mathcal{F}_2^+$ and for the two dissipative slip dicycles $\mathcal{D}_1^+$ and $\mathcal{D}_2^+$ satisfy the simple relation

$$\frac{\Pi_\omega(\mathcal{F}_2^+)\Upsilon(\mathcal{F}_2)}{\Pi_\omega(\mathcal{F}_1^+)\Upsilon(\mathcal{F}_1)} = \frac{\Pi_\omega(\mathcal{D}_2^+)\Upsilon(\mathcal{D}_2)}{\Pi_\omega(\mathcal{D}_1^+)\Upsilon(\mathcal{D}_1)} = \frac{\omega_{57}\omega_{71}}{\omega_{56}\omega_{61}}\frac{(\omega_{61} + \omega_{65})}{(\omega_{71} + \omega_{75})}. \tag{A10}$$

In general, the other two flux ratios (A8) and (A9) between the backward-stepping, dissipative slip, and forward-stepping dicycles $\mathcal{B}^+$, $\mathcal{D}_1^+$, and $\mathcal{F}_1^+$ are lengthy and not very illuminating. However, for the symmetric model with the transition rate constants (A4) and the force-dependent factors (A5), one finds

$$\frac{\Pi_\omega(\mathcal{B}^+)\Upsilon(\mathcal{B})}{\Pi_\omega(\mathcal{F}_1^+)\Upsilon(\mathcal{F}_1)}$$
$$= \frac{\omega_{52}}{\omega_{25}} \times \left(1 + \frac{(\omega_{61} + \omega_{65})\omega_{17}\omega_{75}}{(\omega_{71} + \omega_{75})(\omega_{12}\omega_{65} + \omega_{12}\omega_{61} + \omega_{16}\omega_{65})}\right) \tag{A11}$$

and

$$\frac{\Pi_\omega(\mathcal{D}_1^+)\Upsilon(\mathcal{D}_1)}{\Pi_\omega(\mathcal{F}_1^+)\Upsilon(\mathcal{F}_1)} = \frac{\omega_{12}\omega_{56}\omega_{61}}{\omega_{25}(\omega_{12}\omega_{65} + \omega_{12}\omega_{61} + \omega_{16}\omega_{65})}. \tag{A12}$$

Furthermore, for small product concentrations [ADP] and [P], one obtains the simplified relations

$$\frac{\Pi_\omega(\mathcal{F}_2^+)\Upsilon(\mathcal{F}_2)}{\Pi_\omega(\mathcal{F}_1^+)\Upsilon(\mathcal{F}_1)} = \frac{\Pi_\omega(\mathcal{D}_2^+)\Upsilon(\mathcal{D}_2)}{\Pi_\omega(\mathcal{D}_1^+)\Upsilon(\mathcal{D}_1)} \approx \frac{\omega_{57}}{\omega_{56}}, \tag{A13}$$

$$\frac{\Pi_\omega(\mathcal{B}^+)\Upsilon(\mathcal{B})}{\Pi_\omega(\mathcal{F}_1^+)\Upsilon(\mathcal{F}_1)} \approx \frac{\omega_{52}}{\omega_{25}}, \tag{A14}$$

$$\frac{\Pi_\omega(\mathcal{D}_1^+)\Upsilon(\mathcal{D}_1)}{\Pi_\omega(\mathcal{F}_1^+)\Upsilon(\mathcal{F}_1)} \approx \frac{\omega_{56}}{\omega_{25}}. \tag{A15}$$

[1] I. H. Segel, *Enzyme Kinetics* (Wiley, New York, 1993).

[2] J. Howard, *Mechanics of Motor Proteins and the Cytoskeleton* (Sinauer, Sunderland, 2001).

[3] *Molecular Motors*, edited by M. Schliwa (Wiley-VCH, Weinheim, 2003).

[4] S. Liepelt and R. Lipowsky, Phys. Rev. Lett. **98**, 258102 (2007).

[5] S. Liepelt and R. Lipowsky, Europhys. Lett. **77**, 50002 (2007).

[6] J. Howard, Annu. Rev. Physiol. **58**, 703 (1996).

[7] R. D. Vale, T. S. Reese, and M. P. Sheetz, Cell **42**, 39 (1985); R. D. Vale, *ibid.* **112**, 467 (2003).

[8] N. Hirokawa and R. Takemura, Nat. Rev. Neurosci. **6**, 201 (2005).

[9] L. A. Amos, J. Cell. Sci. **87**, 105 (1987); L. A. Amos and K.

Hirose, *ibid.* **120**, 3919 (2007).

[10] J. T. Yang, W. M. Saxton, R. J. Stewart, E. C. Raff, and L. S. B. Goldstein, Science **249**, 42 (1990).

[11] L. Romberg and R. D. Vale, Nature (London) **361**, 168 (1993).

[12] I. Crevel, A. Lockhart, and R. A. Cross, J. Mol. Biol. **257**, 66 (1996).

[13] W. O. Hancock and J. Howard, J. Cell Biol. **140**, 1395 (1998); Proc. Natl. Acad. Sci. U.S.A. **96**, 13147 (1999).

[14] M. J. Schnitzer and S. M. Block, Nature (London) **388**, 386 (1997).

[15] W. Hua, E. C. Young, M. L. Fleming, and J. Gelles, Nature (London) **388**, 390 (1997).

[16] A. Yildiz, M. Tomishige, R. D. Vale, and P. R. Selvin, Science **303**, 676 (2004).

[17] N. R. Guydosh and S. M. Block, Proc. Natl. Acad. Sci. U.S.A. **103**, 8054 (2006).

[18] M. C. Alonso, D. R. Drummond, S. Kain, J. Hoeng, L. Amos, and R. A. Cross, Science **316**, 120 (2007).

[19] S. M. Block, Biophys. J. **92**, 2986 (2007).

[20] T. Mori, R. D. Vale, and M. Tomishige, Nature (London) **450**, 750 (2007).

[21] R. Subramanian and J. Gelles, J. Gen. Physiol. **130**, 445 (2007).

[22] K. Visscher, M. J. Schnitzer, and S. M. Block, Nature (London) **400**, 184 (1999); M. J. Schnitzer, K. Visscher, and S. M. Block, Nat. Cell Biol. **2**, 718 (2000).

[23] W. R. Schief, R. H. Clark, A. H. Crevenna, and J. Howard, Proc. Natl. Acad. Sci. U.S.A. **101**, 1183 (2004).

[24] N. J. Carter and R. A. Cross, Nature (London) **435**, 308 (2005).

[25] M. Nishiyama, H. Higuchi, and T. Yanagida, Nat. Cell Biol. **4**, 790 (2002); Y. Taniguchi, M. Nishiyama, Y. Ishii, and T. Yanagida, Nat. Chem. Biol. **1**, 342 (2005).

[26] Y.-Z. Ma and E. W. Taylor, J. Biol. Chem. **272**, 724 (1997).

[27] S. P. Gilbert, M. L. Moyer, and K. A. Johnson, Biochemistry **37**, 792 (1998).

[28] D. D. Hackney, Proc. Natl. Acad. Sci. U.S.A. **102**, 18338 (2005).

[29] R. A. Cross, Trends Biochem. Sci. **29**, 301 (2004).

[30] R. Lipowsky and S. Liepelt, J. Stat. Phys. **130**, 39 (2008).

[31] T. L. Hill, *Free Energy Transduction and Biochemical Cycle Kinetics* (Springer, New York, 1989).

[32] U. Seifert, Europhys. Lett. **70**, 36 (2005); Phys. Rev. Lett. **95**, 040602 (2005).

[33] H. Qian, J. Phys.: Condens. Matter **17**, S3783 (2005).

[34] R. A. Alberty, J. Phys. Chem. B **107**, 12324 (2003).

[35] A. W. C. Lau, D. Lacoste, and K. Mallick, Phys. Rev. Lett. **99**, 158102 (2007); D. Lacoste, A. W. C. Lau, and K. Mallick, Phys. Rev. E **78**, 011915 (2008).

[36] F. Jülicher, A. Ajdari, and J. Prost, Rev. Mod. Phys. **69**, 1269 (1997); A. Parmeggiani, F. Jülicher, A. Ajdari, and J. Prost, Phys. Rev. E **60**, 2127 (1999).

[37] S. Liepelt and R. Lipowsky (unpublished).